A multi-layer 'gas of circles' Markov random field model for the extraction of overlapping near-circular objects*

Jozsef Nemeth[1], Zoltan Kato[1], and Ian Jermyn[2]

[1]Image Processing and Computer Graphics Department
University of Szeged, P.O. Box 652, 6701 Szeged, Hungary
[2]Department of Mathematical Sciences, Durham University
South Road, Durham DH1 3LE, United Kingdom

Abstract. We propose a multi-layer binary Markov random field (MRF) model that assigns high probability to object configurations in the image domain consisting of an unknown number of possibly touching or overlapping near-circular objects of approximately a given size. Each layer has an associated binary field that specifies a region corresponding to objects. Overlapping objects are represented by regions in different layers. Within each layer, long-range interactions favor connected components of approximately circular shape, while regions in different layers that overlap are penalized. Used as a prior coupled with a suitable data likelihood, the model can be used for object extraction from images, *e.g.* cells in biological images or densely-packed tree crowns in remote sensing images. We present a theoretical and experimental analysis of the model, and demonstrate its performance on various synthetic and biomedical images.

1 Introduction

Object extraction remains one of the key problems of computer vision and image processing. The problem is easily stated: find the regions in the image domain occupied by a specified object or objects. The solution of this problem often requires high-level knowledge about the shape of the objects sought in order to deal with high noise, cluttered backgrounds, or occlusions [4, 11, 8, 1]. As a result, most approaches to extraction have, to differing degrees and in different ways, incorporated prior knowledge about the shape of the objects sought. Early approaches were quite generic, essentially encouraging smoothness of object boundaries [6, 9, 3, 2, 10]. For example, [10] uses a Markovian smoothness prior (basically a Potts model, *i.e.* boundary length is penalized); [6] uses a line process to control the formation of region boundaries and control curvature; while classical active contour models [9] use boundary length and curvature, and region area in order to favor smooth closed curves [3, 2].

Subsequently there has been a great deal of work on the inclusion of more specific prior shape knowledge in a variational [4, 13] or probabilistic [5, 15] framework. Many of these methods rely on a kind of template matching: shape variability is modeled as

* This research was partially supported by the grant CNK80370 of the National Office for Research and Technology (NKTH) & Hungarian Scientific Research Fund (OTKA).

deformations of a reference shape or shapes. Although these methods are useful for many applications, the major drawback of using a reference shape (or shapes) is that handling an unknown number of instances of an object in the same image is difficult.

An alternative approach, known as 'higher-order active contours' (HOACs), was presented and developed in [11, 7, 8]. HOAC models integrate shape knowledge without using reference shapes via the inclusion of explicit long-range dependencies between region boundary points. The lack of reference shapes means that they can be used to extract multiple instances of the same object. In [8], Horvath *et al.* showed how to set the parameters of the model introduced in [11] to favor regions consisting of any number of approximately circular connected components, each component having approximately the same, specified radius. This 'gas of circles' (GOC) model was successfully used for the extraction of tree crowns from aerial images.

A subsequent reformulation of HOAC models (and active contour models in general) as equivalent phase field models [12, 7] brings a number of theoretical and algorithmic advantages. One of the most important of these is that phase field models can be interpreted as real-valued Markov random fields (MRFs), thereby allowing the theoretical and algorithmic toolbox of random field theory to be brought to bear. In [1], this was carried out, and an MRF GOC model equivalent to the phase field GOC model was developed.

For many important applications, for example the extraction of cells from light microscope images in biology, or the extraction of densely packed tree crowns in remote sensing images, these methods have limitations. The first is due to the representation: distinct overlapping objects cannot be represented. This is because the representation used is of a *region*, *i.e.* a subset of the image domain, and not of objects as such. Thus if the regions corresponding to two objects overlap, they form the single region that is their union. This cannot be distinguished from a single object occupying the same region. The second is due to the model: the same long-range interactions that favor near-circular shapes also introduce a repulsive energy between nearby objects that means that configurations containing nearby objects have low probability, even if they do not overlap.

In this paper, we propose a generalization of the MRF GOC model that overcomes these limitations: the multi-layer MRF GOC model. This consists of multiple copies of the MRF GOC model in [1], each copy being known as a layer. Now overlapping objects *can* be represented, as subsets of two different layers. The layers interact via a penalty for the overlap of regions in different layers, and this inter-layer interaction is crucial, particularly when a likelihood term is added. In its absence, the maximum probability configuration would simply be the same in all layers and equal to that found using the model in [1]. The result is that rather than the regions corresponding to two overlapping objects necessarily merging into a single region, it may be energetically favourable for the two regions corresponding to the two separate objects to appear in different layers.

We begin by recalling the single-layer 'gas of circles' model.

2 The single-layer 'gas of circles' model

The 'gas of circles' model assigns high probability to regions in the image domain consisting of some number of approximately circular connected components, each of which has approximately the same, specified radius, and that are more than a certain distance apart. There are three equivalent formulations of the model: higher-order active contours (HOACs) [8], phase fields [7], and Markov random fields [1]. In the next three subsections, we explain the three formulations, since each provides some insight into the model, and the equivalences between them.

2.1 Contour representation

In the contour formulation, a region R is represented by its boundary ∂R, which is an equivalence class (under diffeomorphisms of their domain) of zero or more closed parameterized curves. The HOAC energy for the GOC model is [8]:

$$E(\gamma) = \lambda_c L(\gamma) + \alpha_c A(\gamma) - \frac{\beta_c}{2} \int n \cdot n' \mathbf{G}(\gamma(t) - \gamma(t'))\, dt\, dt', \tag{1}$$

where the contour γ of length $L(\gamma)$ represents the boundary ∂R of extracted foreground regions with a total area $A(\gamma)$. The last term of Eq. (1) is responsible for the geometry of extracted regions, where n, n' corresponds to the normal vectors at t and t' respectively, while $\mathbf{G}$ is the so called *interaction function*

$$\mathbf{G}(z) = \begin{cases} \frac{1}{2}\left(2 - \frac{\|z\|}{d} - \frac{1}{\pi}\sin\left(\frac{\pi(\|z\|-d)}{d}\right)\right) & \text{if } \|z\| < 2d, \\ 1 - H(\|z\| - d) & \text{otherwise.} \end{cases} \tag{2}$$

where d controls the range of interaction and H is the Heaviside step function. Horvath *et al.* showed in [8], that parameter triples $(\lambda_c, \alpha_c, \beta_c)$ satisfying certain stability conditions will produce circular regions of a given radius r, yielding the first definition of the 'gas of circles' HOAC model.

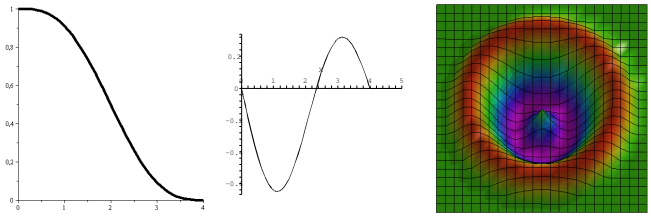

$\mathbf{G}(z)$ $\mathcal{G}(z)$ in 2D $\mathcal{G}(x - x')$ in 3D

Fig. 1. The *interaction function* $\mathbf{G}(z)$ for $d = 2$ and corresponding *geometric kernel* $\mathcal{G}$.

2.2 Phase field representation

The phase field framework represents a region R by a function $\Phi \ni \phi : \mathcal{D} \to \mathbb{R}$ defined on the image domain $\mathcal{D} \subset \mathbb{R}^2$, and a threshold t: $R = \zeta_t(\phi) = \{x \in \mathcal{D} : \ \phi(x) \geq t\}$. The phase field formulation $E(\phi)$ of the contour energy Eq. (1) was described in in [12]:

$$E(\phi) = \int_{\mathcal{D}} \frac{D_f}{2}|\nabla\phi|^2 + \lambda_f\Big(\frac{\phi^4}{4} - \frac{\phi^2}{2}\Big) + \alpha_f\Big(\phi - \frac{\phi^3}{3}\Big) \\ - \frac{\beta_f}{2}\int_{\mathcal{D}\times\mathcal{D}'} \nabla\phi \cdot \nabla'\phi' \ \mathbf{G}(x - x') \ . \quad (3)$$

It is convenient to integrate the non-local term by parts:

$$-\frac{\beta_f}{2}\int_{\mathcal{D}\times\mathcal{D}'} \nabla\phi \cdot \nabla'\phi' \ \mathbf{G}(x - x') = \frac{\beta_f}{2}\int_{\mathcal{D}\times\mathcal{D}'} \phi \, \phi' \ \underbrace{\nabla^2\mathbf{G}(x - x'))}_{\mathcal{G}(x-x')} \ .$$

The value ϕ_R that minimizes $E(\phi)$ for a fixed region R takes the values $+1$ inside R and -1 outside, away from the boundary ∂R, while changing smoothly from -1 to $+1$ in a narrow interface region around ∂R. Basically, the linear operator $\mathcal{G}$ directly acts on the phase field ϕ as a *geometric kernel* (see Fig. 1). In the 'gas of circles' model, the parameters of $E(\phi)$ are adjusted using the contour stability analysis and the equivalence between the formulations so that a circle of the desired radius is stable [7, 8].

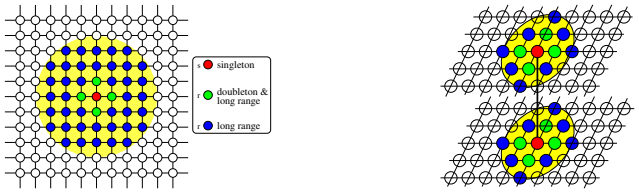

Intra-layer interactions Inter-layer interaction

Fig. 2. MRF neighborhoods.

2.3 Binary MRF representation

Discretizing the field energy Eq. (3) leads to a Markovian interpretation of the phase field model, where ϕ becomes a random field ω taking the discrete values of ± 1 [1]. The resulting energy of the prior distribution $P(\omega)$ is given by

$$U(\omega) = \alpha \sum_s \omega_s + \frac{D}{2}\sum_s \sum_{s' \sim s} (\omega_s - \omega_{s'})^2 + \frac{\beta}{2}\sum_{s,s'} F_{ss'} \ \omega_s \ \omega_{s'} \ , \quad (4)$$

where s denotes lattice sites (or pixels) of the discrete image domain $\mathcal{S}$ and $\sim$ is the nearest neightbour relation. The model parameters are related to the phase field model

by $\alpha = \frac{2\alpha_f}{3}$; $\beta = \beta_f$; while $D = \frac{0.82D_f}{4}$ incorporates the integral over pairs of boundary lattice cells. $F_{ss'}$ is a discrete approximation of $\mathcal{G}$ [1], which also determines the size of the neighborhood: $\{s' \in \mathcal{S} : |s - s'| < 2d\}$ as shown in Fig. 2. The singleton potential $\alpha\omega_s$ of the prior energy corresponds to an area term: a lower α favors more foreground pixels and vice versa, while the doubleton potential $D(\omega_s - \omega_{s'})^2$ acting over a nearest neighborhood of s ensures smoothness by penalizing boundary formation. Finally, the *long-range* potentials enforce the geometric constraints, thereby forming circles:

$$\beta F_{ss'}\,\omega_s\,\omega_{s'} = \begin{cases} -\beta F_{ss'} & \text{if } \omega_s \neq \omega_{s'}, \\ +\beta F_{ss'} & \text{otherwise.} \end{cases} \tag{5}$$

From Fig. 2, it is clear that *long-range* potentials favour the same label when $|s - s'| < d'$ (*attractive* case) and different labels when $d' < |s - s'| < 2d$ (*repulsive* case), where $d' \simeq d$ is the zero of $\mathcal{G}$.

3 The multi-layer MRF 'gas of circles' model

We are now in a position to describe the multi-layer generalization of the MRF GOC model just described. The MRF GOC model has two limitations that render it inappropriate for many applications. First, touching or overlapping objects cannot be represented as separate entities in this model. This is because the representation used is of a region, not of objects as such. If the regions R_1 and R_2 corresponding to two objects overlap, the result is a single region $R = R_1 \cup R_2$ that cannot be distinguished from the representation of a single object occupying the whole of R. Second, the model energy has a sometimes undesirable effect: it discourages connected components from being too close to one another. This is because the same interactions that favor stable circles also produce a repulsive interaction that raises the energy when two circles are closer than $2d$. Thus while this model is able to separate, for example, tree crowns in regular plantations, it cannot represent, nor does it model well, configurations in which objects are touching or overlapping (*cf.* Fig. 8).

The multi-layer MRF GOC model removes both these limitations by using multiple copies of the MRF GOC model, as follows. The domain of the binary random field becomes $\tilde{\mathcal{S}} = \ell \times \mathcal{S}$, or alternatively, the field is a map from $\mathcal{S}$ to $\mathbb{B}^\ell$, where ℓ denotes either $\ell \in \mathbb{Z}^+$ or the set $\{1, \ldots, \ell\}$. Hence $\omega = \{\omega^{(i)}\}$ for $i \in \ell$, where $\omega^{(i)} : \mathcal{S} \to \mathbb{B}$. In principle, we would like $\ell = \mathbb{Z}^+$,*i.e.* an infinite number of layers, as this would place no restrictions on the possible configurations. In practice, there is always a maximum number of mutual overlaps, and ℓ need be no larger than this.

Sites that only differ in the value of i correspond to the same spatial point. Thus $\tilde{\mathcal{S}}$ can be thought of as a series of layers, each of which is isomorphic to $\mathcal{S}$, hence the name 'multi-layer'. It is clear that the multi-layer field can represent overlapping objects, simply by placing the regions corresponding to them on different layers.

The Gibbs energy $\tilde{U}$ of the multi-layer model is the sum of the MRF GOC energies of each layer, plus an inter-layer interaction term that penalizes overlaps (see Fig. 2):

$$\tilde{U}(\omega) = \sum_{i=1}^{\ell} U(\omega^{(i)}) + \frac{\kappa}{4} \sum_{i \neq j} \sum_{s} (1 + \omega_s^{(i)})(1 + \omega_s^{(j)}) \,, \tag{6}$$

where κ is a new parameter controlling the strength of the overlap penalty.[1] Note that the inter-layer energy is ultralocal: only corresponding sites on different layers interact. Thus two regions in different layers experience no interaction at all unless they overlap. This eliminates the repulsive energy that exists in the single-layer model, because nearby but non-overlapping regions in different layers always have lower energy than the same regions in the same layer, assuming the intra-layer interactions are repulsive.

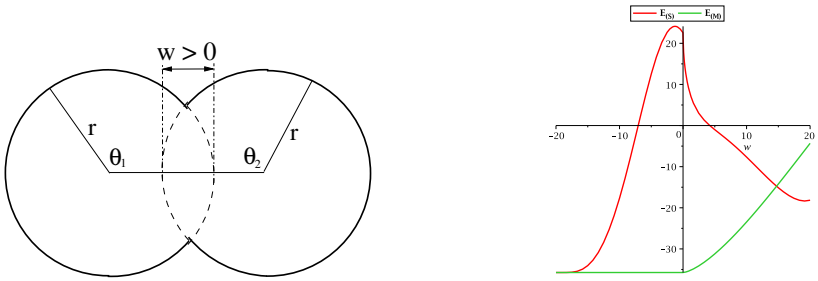

Fig. 3. Configurations of two overlapping circles and corresponding plots of $E_{(M)}(r, w)$ and $E_{(S)}(r, w)$ vs. w for two circles of radius $r = 10$.

3.1 Energy of two interacting circles

In order better to understand the behaviour of the model, in this section we analyze the energy of two circles, on the same layer and on different layers. We consider the configurations shown in Fig. 3, where w stands for the size of the intersection: $w < 0$ means the circles do not intersect, while $w > 0$ represents a non-empty intersection of width w. We want to express the energy of these configurations as a function of w. We take advantage of the equivalence of the 'gas of circles' MRF and HOAC models to use the higher-order active contour energy Eq. (1) to compute the energy of the two circles. The parameters of this energy come from the equivalences between the three formulations: $\beta_c = 4\beta$; the unit weight of a boundary point is $\frac{4D}{0.82}$; while the difference in energy between an interior and exterior point is 2α. Thus the MRF energy of a single circle with radius r can be written as

$$E(r) = \frac{4D}{0.82} 2\pi r + 2\alpha\pi r^2 - 2\beta \iint_0^{2\pi} d\theta \, d\theta' \, r^2 \cos(\theta - \theta') \, G(\gamma(\theta) - \gamma(\theta')) \, , \quad (7)$$

where γ is an embedding corresponding to the circle, parameterized, as shown in Fig. 3, by polar angle θ.

[1] Notice that $\tilde{U}$ is invariant to permutations of the layers. This will remain true even after we add a likelihood energy. Thus all configurations, and in particular minimum energy configurations, are $\ell!$ times degenerate. In practice, this degeneracy will be spontaneously broken by the optimization algorithm.

Different layers: When the two circles are in different layers, the only interaction energy is the inter-layer overlap penalty. Thus the energy is constant until the circles start to overlap. It then starts to increase:

$$E_{(M)}(r,w) = 2E(r) + \kappa A(r,w) \ , \tag{8}$$

where $A(r,w)$ is the area of the overlap given by

$$A(r,w) = \begin{cases} 2\left(r^2 \arccos\left(1-\frac{w}{2r}\right) - \left(r-\frac{w}{2}\right)\sqrt{2rw-\frac{w^2}{4}}\right) & \text{if } w>0, \\ 0 & \text{otherwise.} \end{cases} \tag{9}$$

Same layer: When the two circles are in the same layer, they interact if $w > -2d$ for the particular form of interaction function in Eq. (2). (Note that we need only consider $w \leq 2r$, where r is the radius of the circles, due to symmetry.) Thus if $w \leq -2d$, the energy is simply $2E(r)$. For $w > -2d$, the energy increases with w until $w \cong 0$. As the circles start to overlap (and thus no longer form two circles, but a combined 'dumbbell' shape), there is effectively an attractive energy that causes an energy decrease with increasing w until the combined shape, and thus the energy, becomes that of a single circle ($w = 2r$). More precisely, the energy of two circles is

$$\begin{aligned} E_{(S)}(r,w) = {} & \frac{4D}{0.82} 2(2r\pi - L(r,w)) + 2\alpha(2r^2\pi - A(r,w)) \\ & - 4\beta \iint_{\theta_s}^{\theta_f} d\theta_1 \, d\theta_1' \, r^2 \cos(\theta_1 - \theta_1') \, G(\gamma_1(\theta_1) - \gamma_1(\theta_1')) \\ & - 2\beta \iint_{\theta_s}^{\theta_f} d\theta_1 \, d\theta_2 \, r^2 \cos(\theta_1 - (\pi - \theta_2)) \, G(\Delta(\theta_1,\theta_2,w)) \ , \end{aligned} \tag{10}$$

where $\gamma_{1,2}$ are two embeddings corresponding to the two circles, parameterized by angles $\theta_{1,2}$ respectively, as shown in Fig. 3. We have taken advantage of symmetry to write the second line in terms of γ_1 only. $L(r,w)$ is the arc length of the intersection segment, while

$$\Delta(\theta_1,\theta_2,w) = \sqrt{(r(\sin(\theta_1)-\sin(\theta_2)))^2 + (2r - w - r(\cos(\theta_1)-\cos(\theta_2)))^2} \tag{11}$$

is the distance between the points $\gamma_1(\theta_1)$ and $\gamma_2(\theta_2)$. The limits $\theta_s = \cos^{-1}(\min(1, \frac{1-w}{2d}))$ and $\theta_f = 2\pi - \theta_s$ are the radial angles of the two intersection points.

The righthand side of Fig. 3 shows plots of $E_{(M)}(r,w)$ and $E_{(S)}(r,w)$ against w for circles with $r = 10$. When the overlap is greater than a certain threshold, controlled by κ, the energy of two circles in different layers becomes greater than two partially merged circles in one layer. Below this threshold, the two layer configuration has a lower energy. The stable configuration energy of two circles is given by the lower envelope of the curves in Fig. 3, and thus the repulsive energy that exists in the single-layer MRF GOC model is eliminated in the multi-layer MRF GOC model.

4 Experimental results

In this section, we report on the quantitative evaluation of the behavior and performance of the multi-layer MRF GOC model in object extraction problems involving simulated data and microscope images. Results were obtained as MAP estimates, using the multi-layer MRF GOC model as a prior, combined with a likelihood energy U_L to be described shortly: $\hat{\omega} = \arg\max_\omega P(I|\omega)P(\omega) = \arg\min_\omega U_L(I,\omega) + \tilde{U}(\omega)$, where $I : \mathcal{S} \to \mathbb{R}$ is the image data. Optimization was performed using Gibbs sampling coupled with simulated annealing [6]. The annealing schedule was exponential, with half-life at least 70 iterations, and a starting temperature of 3.0 for the parameter values used in the experiments.

4.1 Data likelihood

The data likelihood models the image in the interior and exterior regions using Gaussian distributions with constant means, and covariances equal to different multiples of the identity. In addition, we add an image gradient term connecting neighboring pixels, as follows. For each pair of neighboring sites, s and s', let (s, s') be the unit vector pointing from s to s'. Let $\hat{s} = \arg\max_{t\in\{s,s'\}}(|\nabla I(t)|)$. Let $h(s, s') = |(s, s') \cdot \nabla I(\hat{s})|$. Then define

$$g_i(s,s') = \begin{cases} h(s,s') & \omega_s^{(i)} = \omega_{s'}^{(i)}, \\ |\nabla I(\hat{s})| - h(s,s') & \text{otherwise.} \end{cases} \tag{12}$$

The likelihood energy then becomes

$$U_L(I,\omega) = \sum_i \gamma \left\{ \sum_s \left[\ln\left((2\pi)^{1/2}\sigma_{\omega_s^{(i)}}\right) + \frac{\left(I_s - \mu_{\omega_s^{(i)}}\right)^2}{2\sigma^2_{\omega_s^{(i)}}} \right] + \frac{\gamma_2}{2} \sum_s \sum_{s'\sim s} g_i(s,s') \right\}, \tag{13}$$

where γ and γ_2 are positive weights. In practice, the parameters $\mu_{\pm 1}$ and $\sigma_{\pm 1}$ of the Gaussian distributions were learned from representative samples.

4.2 Simulation results with the multi-layer MRF GOC model

In the first experiment, we study the global minima of $\tilde{U}$. Choosing, wlog, $d = 10$, with the intra-layer parameters $\alpha = 0.18634$, $D = 0.15451$, and $\beta = 0.091137$ set according to the stability constraints [8, 1] and to ensure that stable circles have negative energy, $\tilde{U}$ was then minimized for different numbers of layers ℓ and values of κ. Fig. 4 shows representative examples of these optimal configurations. The top-left result has $\ell = 1$: note the spacing of the circles due to the intra-layer repulsive energy. When there are more layers, the intra-layer energies favour a similarly dense 'gas of circles' in each layer. For $\ell \leq 3$, every layer may contain such a configuration without the circles in different layers overlapping. For $\ell > 3$, it is not possible to achieve both an optimal configuration in each layer and zero overlap energy. For small κ, the model tries to generate a dense configuration in each layer at the price of having overlaps. For large κ, the situation is the opposite: the model tries to avoid overlaps at the price of having

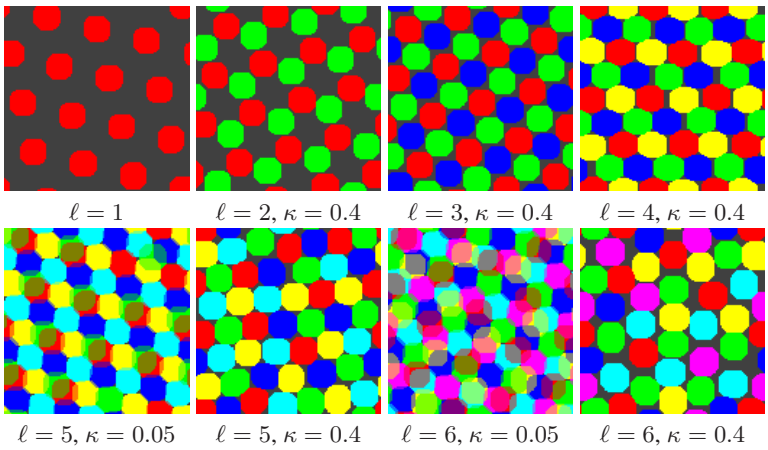

Fig. 4. Stable configurations of the multi-layer MRF GOC model for different numbers of layers and values of κ.

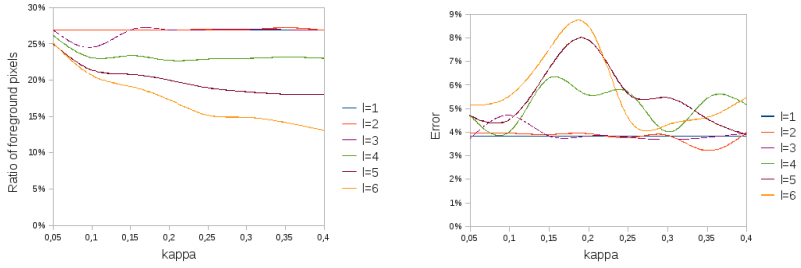

Fig. 5. Plots of the relative interior area (left) and shape error (right) of the stable configurations against κ.

less circles in each layer. Fig. 5 shows a plot of the relative interior area $\frac{1}{\ell N}\sum H(\omega)$ against κ, where $N = |\mathcal{S}|$. The value is almost constant for $\ell \leq 3$, while for $\ell > 3$, the value decreases with κ. The circularity of the regions was also evaluated. The righthand plot in Fig. 5 shows the percentage of pixels outside the ideal desired circles. Although for $\ell > 3$, these errors increase slightly, overall they remain low, meaning that the connected components remain circles to good accuracy for all ℓ and κ.

4.3 Quantitative evaluation on synthetic images

In this experiment, we demonstrate the efficiency of our model in separating overlapping circles. A series of noisy synthetic images were generated containing two circles of radius 10 with different degrees of overlap. The weights in the likelihood energy were set to $\gamma = 0.1$ and $\gamma_2 = 0$, *i.e.* no gradient term was used. We used two layers and differing κ values in the range $[0.01, 1]$. Segmentation error was evaluated as the proportion of incorrectly segmented pixels. A plot of these errors versus the amount of overlap w and κ is shown in Fig. 6. Note that there is a rather clear drop in the segmentation error for $\kappa \cong 0.7$. When $w > 10$ (corresponding to an overlap of greater than 50%), a larger κ is required to get an accurate segmentation ($\kappa = 0.88$ was needed in the last case in Fig. 6), and for $w > 15$, it is hard to get good quality results. In summary, the model performs well for reasonable overlaps and it is not sensitive to the value of κ. On the other hand, there is a performance drop for very large overlaps.

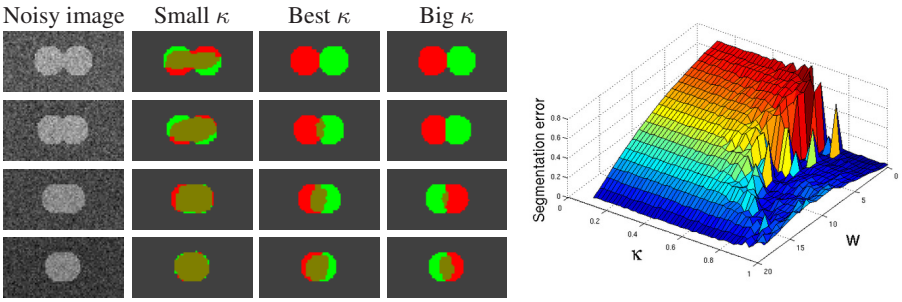

Fig. 6. Results on noisy synthetic images (SNR= 0dB) containing two circles of radius 10 with different degrees of overlap. Left: typical extraction results. Right: plot of segmentation error as a function of degree of overlap (w) and κ.

4.4 Application in biomedical imaging

Biomedical image segmentation aims to find the boundaries of various biological structures, *e.g.* cells, chromosomes, genes, proteins and other sub-cellular components in various image types [14]. Light microscope techniques are often used, but the resulting

images are frequently noisy, blurred, and of low contrast, making accurate segmentation difficult. In many cases, the geometric structures involved are near-circular with many overlaps, so that our model seems well suited to extracting the desired structures. The extraction results shown in Fig. 7 and Fig. 8 demonstrate the effectiveness of the proposed multi-layer MRF GOC model for this type of task. Computation times vary from $\sim$ 20s to $\sim$ 1000s for images of size $N = 10^4$. The key factor is the number of layers, with the minimum time corresponding to $\ell = 2$, the maximum to $\ell = 6$.

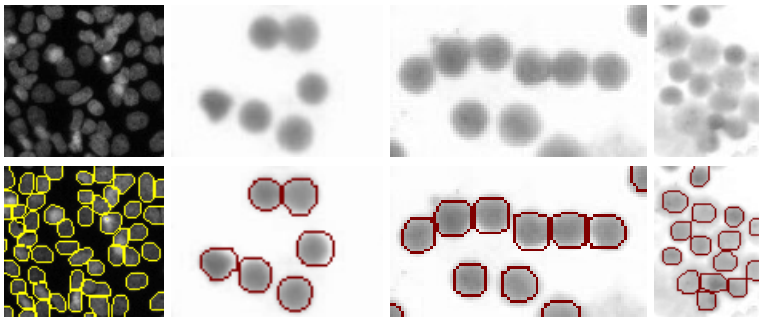

Fig. 7. Extraction of cells from light microscope images using the multi-layer MRF GOC model.

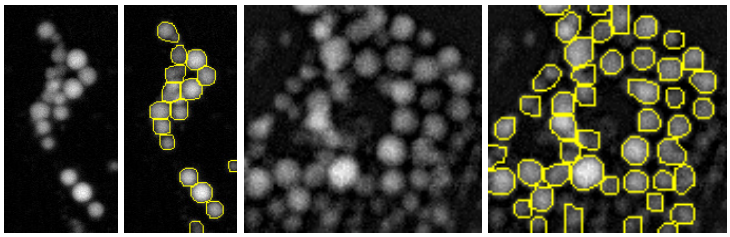

Fig. 8. Extraction of lipid drops from light microscope images using the multi-layer MRF GOC model.

5 Conclusion

The multi-layer MRF GOC model enables the representation and modeling of object configurations consisting of an *a priori* unknown number of approximately circular objects of roughly the same size, which may touch or overlap. Such configurations occur in a number of domains, notable biomedicine and biology (*e.g.* cell images), and remote sensing (*e.g.* images of closely planted trees). Experiments show that the model

behaves as expected on theoretical grounds, and that, when coupled with an appropriate likelihood model, can successfully extract such object configurations from synthetic and real images. The multi-layer model should also enable the extraction of several sets of approximately circular objects of different sizes, by setting the model parameters differently on different layers of the model.

References

1. Blaskovics, T., Kato, Z., Jermyn, I.: A Markov random field model for extracting near-circular shapes. In: Proceedings of International Conference on Image Processing. pp. 1073–1076. IEEE, IEEE, Cairo, Egypt (Nov 2009)
2. Caselles, V., Kimmel, R., Sapiro, G.: Geodesic active contours. International Journal of Computer Vision 22(1), 61–79 (1997)
3. Cohen, L.: On active contour models and balloons. Computer Vision, Graphics and Image Processing: Image Understanding 53, 211–218 (1991)
4. Cremers, D., Tischhauser, F., Weickert, J., Schnorr, C.: Diffusion snakes: Introducing statistical shape knowledge into the Mumford-Shah functional. International Journal of Computer Vision 50(3), 295–313 (2002)
5. Flach, B., Schlesinger, D.: Combining shape priors and MRF-segmentation. In: Proceedings of the 2008 Joint IAPR International Workshop on Structural, Syntactic, and Statistical Pattern Recognition. vol. 5342, pp. 177–186. Lecture Notes In Computer Science, Orlando, Florida (2008)
6. Geman, S., Geman, D.: Stochastic relaxation, Gibbs distributions and the Bayesian restoration of images. IEEE Transactions on Pattern Analysis and Machine Intelligence 6, 721–741 (1984)
7. Horvath, P., Jermyn, I.H.: A 'gas of circles' phase field model and its application to tree crown extraction. In: Proceedings of European Signal Processing Conference (EUSIPCO). Poznan, Poland (Sep 2007)
8. Horvath, P., Jermyn, I., Kato, Z., Zerubia, J.: A higher-order active contour model of a 'gas of circles' and its application to tree crown extraction. Pattern Recognition 42(5), 699–709 (May 2009)
9. Kass, M., Witkin, A., Terzopoulos, D.: Snakes: Active contour models. International Journal of Computer Vision 1(4), 321–331 (1988)
10. Kato, Z., Berthod, M., Zerubia, J.: A hierarchical Markov random field model and multi-temperature annealing for parallel image classification. Computer Vision, Graphics and Image Processing: Graphical Models and Image Processing 58(1), 18–37 (Jan 1996)
11. Rochery, M., Jermyn, I.H., Zerubia, J.: Higher order active contours. International Journal of Computer Vision 69(1), 27–42 (August 2006), http://dx.doi.org/10.1007/s11263-006-6851-y
12. Rochery, M., Jermyn, I.H., Zerubia, J.: Phase field models and higher-order active contours. In: Proc. IEEE International Conference on Computer Vision (ICCV). Beijing, China (October 2005)
13. Rousson, M., Paragios, N.: Shape priors for level set representations. In: Proc. of European Conference on Computer Vision. pp. 78–92. Lecture Notes in Computer Science, Springer, Copenhagen, Denmark (2002)
14. Russell, C., Metaxas, D., Restif, C., Torr, P.: Using the P^n Potts model with learning methods to segment live cell images. In: IEEE 11th International Conference on Computer Vision. pp. 1–8. IEEE (October 2007)
15. Srivastava, A., Joshi, S., Mio, W., Liu, X.: Statistical shape analysis: Clustering, learning, and testing. IEEE Trans. Pattern Analysis and Machine Intelligence 27(4), 590–602 (2005)